JOURNAL OF OPTOELECTRONICS AND ADVANCED MATERIALS Vol. 11, No. 3, March 2009, p. 338 - 347

Carbon nanotubes from ethanol on Fe-Co/MgO catalysts and related interface phenomena

D. LUPU, A. R. BIRIŞ, I. BALTOG[a], M. BAIBARAC[a], V.KUNCSER[a], G. SCHINTEIE[a], M. VALEANU[a], S. LEFRANT[b], A.S. BIRIS[c], I. MIŞAN, G. FILOTI[a*]
National Institute for R&D of Isotopic and Molecular Technologies, Cluj-Napoca, Romania
[a]*National Institute for R&D of Materials Physics, Bucharest, Romania*
[b]*Institut des Matériaux Jean Rouxel, Laboratoire de Physique Cristalline, Nantes, France*
[c]*Applied Science Department, University of Arkansas at Little Rock, AR, USA*

Mössbauer spectroscopy studies of Fe-Co/MgO catalysts proved that a high dispersion degree of Fe may be achieved for catalysts containing Fe/Co in a ratio close to 1. During materials processing. the presence of hydrogen at high temperatures, even for short time, induced an increased particle size of the catalytic Fe. The evaluation of various iron species from their areas in the Mössbauer spectra revealed the dependence of the nanotube amount on (FeCo alloy + Fe^{2+}) content in the catalyst, in good agreement with literature mechanisms. The Raman spectra show that carbon nanotubes synthesized from ethanol in argon flow on 4.5%Fe:4.5%Co/MgO are richer in low diameter (0.7-1.0nm) tubes than those obtained at low ethanol pressure, in agreement with the effects of hydrogen reported in literature. The close similarity with the Raman spectra of Aldrich double-walled carbon nanotubes and from literature, recommends the syntheses in argon flow as better conditions for double-walled carbon nanotube growth.

(Received January 15, 2009; accepted March 19, 2009)

Keywords: Carbon nanotubes, Fe-Co/MgO catalyst, Mossbauer spectroscopy

1. Introduction

The synthesis of carbon nanotubes from alcohols on Fe-Co/zeolite catalysts, introduced by Maruyama *et al.* [1], proved to result in high quality Single Wall carbon nanotubes (SWNTs), almost free of amorphous carbon [1-8]. Various reaction conditions (temperature, catalytic metal loading on the support, low pressure or atmospheric, pre-activation of the catalyst, residence time) the formation of single (SWNTs), double (DWNTs), multi-wall nanotubes (MWNTs) forms. In the last years efforts to improve the selectivity and yield of the nanotubes synthesized on solid state catalysts via Chemical Catalytic Vapour Deposition (CCVD) method were oriented in a search for new catalysts and adjusting the reaction conditions in close correlation with the factors affecting the size of the catalytic nanoparticles, critical for the growth of different nanotube types among which the DWNTs are of particular interest [9]. The reason for growing a mixture of DWNTs and SWNTs lies in their very similar catalytic growth conditions, including the high homogeneity distribution of metal particles [10].

MgO is a very attractive support, as it can be removed from the products by non-oxidizing acids like HCl without damaging the nanotubes [11]. Moreover, the reduced iron can be better dispersed on MgO than on Al_2O_3 and SiO_2 [12] which should be an advantage for the formation of small catalytic nanoparticles. Ago *et al.* [13] proved the role of strong metal-support interactions in the formation of small size metal nanoparticles, suitable for SWNT(DWNT) synthesis on Fe/MgO catalysts and proposed a mechanism based on the observation that the dispersion of Fe^{3+} ions into MgO bulk is favoured by the catalyst pre-treatment in argon at high temperature while the presence of hydrogen increases the particle size and suppresses the nanotube growth. A detailed investigation by Coquay et al. [14] of Fe/Co-MgO catalyst by Mössbauer spectroscopy revealed that Co ions readily substitute for Mg in MgO lattice, which hinders the dissolution of iron. Upon reduction with hydrogen, the well dispersed Fe^{3+} ions in MgO tend to form Fe^{2+}, resistant to some extent against further reduction to metallic iron. The well dispersed Fe^{3+} ions and the existence of small $MgFe_2O_4$-like particles lead to efficient catalytic metal particles, while the iron rich Fe-Co system activated by Co, favours the growth of carbon nanotubes (mostly SWNTs and DWNTs) [14].

In this paper, the various iron species appeared on MgO supported catalysts are studied by Mössbauer spectroscopy in order to correlate the type of nanotubes resulted from ethanol with the above mentioned mechanisms and roles [13,14]. Because the type of nanotubes strongly depends on the CCVD conditions, the ways to increase the DWNTs content have been also investigated by Raman Spectroscopy.

2. Experimental

The CCVD syntheses were performed in an induction heating set up described elsewhere in detail [15,16] using a quartz tube of 18 mm inner diameter. The pretreatments in argon (10% H_2) for Mössbauer spectroscopy were

performed in the same tube. For CCVD in vacuum, 20-40 mg catalyst was disposed on a graphite cylinder of 12 mm outer diameter (10 mm inner diameter) was heated inductively at 400°C for 40 min in argon (10% H_2), then pumped to vacuum. When the pressure decreased down to 10^{-2} Torr, the ethanol was released in the system through suitable valves, keeping a constant ethanol pressure of 5 Torr while concomitantly increasing the temperature to 900°C. After 15 min the ethanol flow was stopped and the high frequency inducing oven was turned off, cooling the catalyst-holder ensemble in pure argon flow.

The controlled ethanol flowing was settled to 0.027g/min. For syntheses in argon (without hydrogen), after the activation stage in the same conditions as above, the hydrogen from argon was cut off, the temperature was increased to 900°C and the ethanol flow was ensured by bubbling a measured part of the argon through ethanol at room temperature, again for 15 min. It should be noted that the so called activation stage at 400°C still does not lead to the complete reduction of iron species as shown below by Mössbauer spectroscopy.

The fitting procedure consists of a non-linear regression method using Lorentz line shapes and one common line-width per pattern. The temperature dependent Mössbauer measurements have been performed via a liquid nitrogen bath cryostat between 77 K and 300 K. The linear symmetrical wave-form mode of the velocity was utilized. The ^{57}Co source in Rhodium matrix had an average activity of around 1 GBq. A α-Fe foil was used for calibration, and the isomer shift is permanently referred to it. The absorber powder was stacked in a Cu holder, strongly pressed between two mica foils. The thickness of the absorber was of about 10 mg Fe/cm^2.

The Raman spectra were obtained using the surface-enhanced Raman scattering technique (SERS) that operates with 10^2-10^4 enhanced Raman signals. Gold films of 60-150 nm thickness were used as SERS supports. The Raman spectra were recorded in a backscattering geometry using a FT Bruker RFS 100 Spectrometer working at λ_{exc} = 1064 nm , a Jobin-Yvon Horiba T64000 or LabRAM HR 800 Micro Raman Spectrometer for λ_{exc}= 676.4 , 632.8 and 514.5 nm, all equipped with a microprobe allowing to focus the laser beam on the sample within a one micron scale.

3. Results and discussion

3.1 Correlation with the nanotube growth mechanisms

The characteristics of nanotubes synthesized by CCVD strongly depend on the particle size of catalytic metal while the presence of hydrogen plays a dominant role in the development of metal nanoparticles on the catalyst surface. The reduction to metallic state may result either by an activation procedure in hydrogen or even during the CCVD via H_2 resulting from the decomposition of the carbon source.

3.1.1 Mössbauer spectroscopy on pre-treated catalysts

Even without a pre-activation treatment in hydrogen to reduce the iron species, H_2 produced during the CCVD process may increase the nucleation size of catalytic metal particles [13] and information on the effect of H_2 on the various Fe species in any particular catalyst is therefore useful for subsequent selective syntheses. Hydrogen was not introduced during the CCVD syntheses reported here from ethanol but it can arise from the ethanol decomposition (in the absence of water, at 800-900°C up to 3moles H_2/mole of ethanol [17] are released).

The Mössbauer studies on the catalysts after various pre-treatment in argon flow with 10% H_2 were performed in order to investigate the effect of hydrogen on the evolution of different oxidation states: such as the reduction of Fe^{3+} to Fe^{2+} and formation of Fe-Co alloy. The identification of the reduced states of iron (and their amount), induced via hydrogen presence, is important for their relationships with the CCVD mechanism on Fe:Co/MgO catalysts as reported in literature [13,14].

Two catalysts have been studied: 4.5%Fe:4.5%Co/MgO (abbreviated 78) and 2.5%Fe:1.25%Co/MgO (79), after the following pre-treatments followed by cooling to room temperature: 78-N 1h at 400° C in argon flow with 10% H_2; 78-A and 79-A 1h at 400 °C in argon flow with 10% H_2 then heated 2 min at 900 °C.

The sample 78-I is the CCVD product after dissolution of the catalyst by Soxhlet extraction in HCl 24 h, still contain encapsulated around 9.3% FeCo.

The Mössbauer spectra are presented in two figures with Fig. 1 showing the patterns for as prepared sample 78-N and the Fig. 2 showing the other four spectra for reason of easy visual comparison and understanding. The parameters describing various Fe species are grouped in table 1.

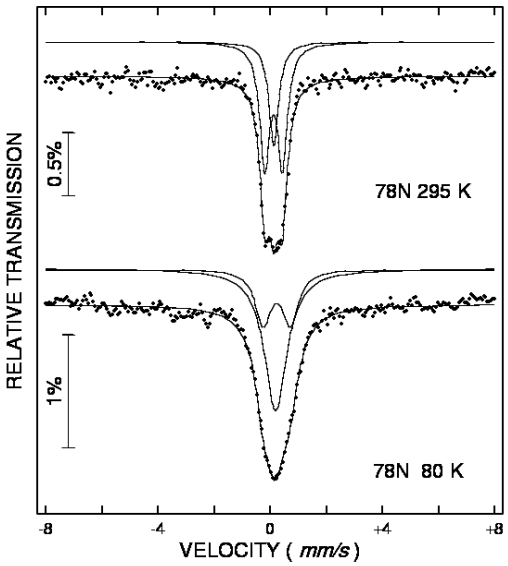

Fig. 1. Mössbauer spectra for catalysts 78-N at two different temperatures 80 and 295 K

Table 1 proves unambiguously the usefulness of measurements at two different temperatures. For example sample 78-N measured at room temperature (RT = 295 K) shows narrower lines and due to lower interactions a stronger superposition of patterns. The Mössbauer measurement at 80 K provides information about an increased distortion evidenced both by larger quadrupole splitting of the doublet as well as a noticeable (Fig. 1) larger line width for singlet. That could primarily be interpreted as a result of a low dimensionality of resulted grains (a super-paramagnetic state), with a rather broad range of dimension, but also as an evidence of more stronger interactions.

In this context the central line in spectra contains also some collapsing sextets (spins are not completely blocked at 80 K) appearing as magnetic ordered phase (see Fig.2 and Table 1) in the other samples at the same temperature. The singlet represents an intimate Fe-Co compound , with high symmetry (HS in Table 1) of iron surroundings while the parameters of the doublet plead for Fe^{3+} species as markedly mentioned in the last column of table containing the Mössbauer parameters. The evolution of pattern area at the mentioned two temperatures denotes a clear fingerprint of strong difference in the Debye temperatures of the involved species, standing for un-equivalent lattice vibrations. Compared with other samples, 78 –N clearly contains smaller particles and an homogeneous dispersion of Fe^{3+} in MgO lattice as well as a result of only one hour treatment in argon ($10\%H_2$) does not completely transform all Fe^{3+} to the reduced Fe^{2+} state.

Table 1. Mössbauer parameters at 80 K or room temperature for samples 78 (N and A type) as well as for 79 and 78

Sample	Area (%)	IS or ε (mm/s)	QS (mm/s)	B_{eff} (T)	Species
78-N RT	30.3	0.13	0.00	0.0	Fe-Co
	69.7	0.14	0.64	0.0	Fe^{3+}
78-N 80K	34.0	0.20	0.00	0.0	Fe-Co
	66.0	0.25	0.98	0.0	Fe^{3+}
78-A RT	12.2	0.05	-0.02	36.5	Fe-Co
	9.8	0.02	0.14	34.4	Fe-Co
	48.0	0.20	0.82	0.0	Fe^{3+}
	26.4	1.01	0.78	0.0	Fe^{2+}
	3.6	1.10	1.68	0.0	Fe^{2+}
78-A 80 K	18.2	0.14	0.06	37.0	Fe-Co
	6.2	0.13	-0.11	34.5	Fe-Co
	40.6	0.29	0.59	0.0	Fe^{3+}
	20.5	1.27	1.16	0.0	Fe^{2+}
	14.5	1.23	1.98	0.0	Fe^{2+}
79-A 80 K	13.9	0.10	0.11	38.9	Fe-Co
	21.9	0.11	0.14	35.0	Fe-Co
	19.7	0.31	0.92	0.0	Fe^{3+}
	38.1	0.85	0.97	0.0	Fe^{2+}
	6.4	1.10	1.36	0.0	Fe^{2+}
78-I 80 K	32.1	0.14	0.00	36.7	Fe-Co
	62.3	0.15	0.00	34.5	Fe-Co
	2.6	0.25	0.38	0.0	Fe^{3+}
	3.0	-0.05	0.00	0.0	Fe-Co s.p.

The sample 78-A which was treated in hydrogen at 900°C for 2 min explicitly proved the reducing effect via presence of Fe^{2+} species in Mössbauer spectra.

The evolution of parameters points to more emphasized effects at lower temperatures. The amounts of Fe^{3+} and Fe^{2+} remain comparable at both temperatures due to closed Debye temperatures of the involved species. There is a smaller amount of Fe-Co compound showing a value close to a quarter of total area of the spectrum. The magnetically ordered phase represents a Fe-Co solid solution conserving the body centered cubic structure of alpha iron phase. As expected the presence of Co in the neighborhood of Fe increased the effective field (B_{eff}) at nucleus on both iron coordination as derived from the parameters of ordered phase displayed in the Table 1. Lowering the temperature, the sample 78-A spectra are showing larger distribution of Fe^{2+} ion sites (via increased line width) and local distortion (larger quadrupole splitting), similar to mentioned behaviour of the sample 78-N spectra.

In the sample 79-A, similar to 78-A, the iron ions are showing the same species but with a noticeable higher amount of Fe-Co and lower one for Fe^{3+} and a less distorted surroundings for Fe^{2+}, also in larger amount, which suggest a smaller penetration of iron into MgO

support, this making it more accessible to reduction with hydrogen in 2 min la 900°C.

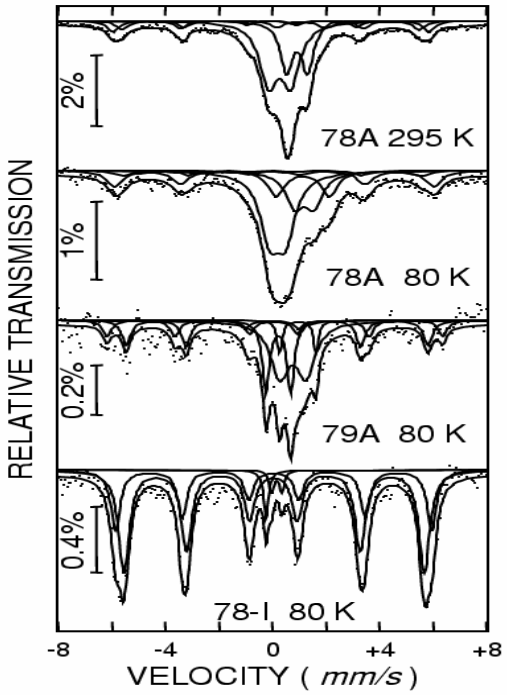

Fig.2 The Mössbauer spectra of samples 78-A, 78-I and 79-A

The picture with the presence of non-reduced Fe^{3+} bonded to oxygen is in agreement with literature [14] mentioning a high resistance at hydrogen reduction of such catalysts.

A careful scrutiny of data emphasizes the role played by the amount of metals (Fe+Co) dispersed on MgO substrate. The Fe-Co alloys appeared with higher percentage from total iron as compared to 78A sample.

Grains of order of one micron could be considered when magnetic phases are put in evidence in Mössbauer spectra close to room temperature and of a noticeable reduced dimensionality when appears only at 80 K.

Finally, the spectra for 78-I show mainly characteristic sextets of Fe-Co alloy, again with Fe accommodating in two different positions, as previously discussed, which pleads for stability of the Fe-Co inter-metallic solution, probably encapsulated, located at the end in the nanotube as the nanotubes grow on these particles. There are small amount of Fe^{3+} arising from catalyst particles covered by the nanotube bundles, not dissolved in acid during the first purification stage.

The values and temperature behaviour of dynamic Mössbauer parameters (line-widths and area mainly), suggests that the grains contain simultaneously large metallic particles and small size metal and oxide ones, showing both super-paramagnetic state, the dimension of the latter being influenced by their direct interaction with carbon nanotubes.

It has to be mentioned, based on above presentation that Fe-Co particles ≥7 nm grow during CCVD because no such particles appeared for a treatment of 1h in argon(10% H_2) as before shown .

3.2 Correlation between the nanotube yield and the previously accepted mechanisms quoted in the literature

The yield of carbonaceous products η (in weight %) obtained for the two samples are: η(78)=17% and η(79)=12% related to the overall catalyst weight. The values related to the content of catalytic metal Fe or (Fe+Co) are also given in Table 2 but they do not fit to the overall yield ratios. The question arises which could be the major species implied in the CCVD process. It seems interesting to calculate the yields / species amount normalized with their relative fraction obtained from the area of the specific patterns appearing in the Mössbauer spectra (e.g. for Fe in Fe-Co alloy, as Fe^{2+} or their sum) as given below.

Table 2. The yield of carbonaceous products normalized to various iron species for the samples 78 and 79

sample	η/ total catalyst	η/ Fe in catalyst	η/ (Fe+Co) in catalyst	η/ Fe-Co alloy area	η/ Fe^{2+} area	η/ (Fe-Co)+ Fe^{2+} area
78	17	378	189	1718	1260	727
79	12	480	320	1340	1078	598

It is interesting to note that only the yields normalized to Fe-Co, Fe^{2+} or to their sum show a higher relative yield 78/79 as is the case.

This is in agreement with the models proposed by Coquay *et al.* [14]. It is quite reasonable to refer the yield to the sum of Fe-Co alloy (directly implied in the nanotube growth) plus Fe^{2+} ions (potential precursor of Fe-Co particles) according to the literature proposed models [13,14]. The iron appeared as Fe^{2+} species following the samples treatment, as was evidenced from Mössbauer measurements, reveals that all Fe^{3+} are easily available for reduction in sample 79, more or less close to the surface, showing also a poor dispersion.

As compared to sample 78, the diminishing of Co/Fe ratio in 79 proves to be less favourable for high quality SWNTs, which is indeed the case as evidenced below by the Raman spectra of the carbon nanotubes. The chemical analysis of the encapsulated metal revealed the overall composition $Fe_{0.53}Co_{0.47}$ in the nanotubes 78 of better quality and $Fe_{0.73}Co_{0.27}$ for 79, in agreement with the

observations of Coquay et al. [14] that Co^{2+} hinders the dissolution of iron in MgO and favours the formation of Fe-Co particles of size and composition close to $Fe_{0.50}Co_{0.50}$ adequate for CNT formation.

The Mössbauer spectroscopy results proved to be a very useful tool providing parameters for calculating the yields of carbon nanotubes related to various iron species co-existing in the catalyst and also to evaluate their role in the growth process and the quality of the obtained carbon nanotubes. The chemical analysis of encapsulated metal and the characteristics of the nanotubes obtained on two different catalysts suggest that at low Co content, the rate of Co transfer from the bulk MgO to the catalyst surface, where the nanotubes growth takes place, has a detrimental effect on the quality of nanotubes.

4. Comparative Raman spectroscopic characterization of the products

4.1 The Raman spectrum of carbon nanotubes

Some information concerning the carbon nanotubes and their vibration properties are necessary to be reminded, before to develop the topic. A SWNT is a grapheme sheet rolled up into a cylinder with both ends capped with hemispheres made of hexagonal and pentagonal carbon rings. Regardless of the synthesis method, microscopic studies have revealed that samples consist of bundles of 20-100 individual nanotubes aligned in a two-dimensional crystal packing arrangement over essentially their entire length [18]. The bundles, also known as nano-ropes, contain both metallic and semiconducting tubes. Raman spectroscopy is one of the most used technique in the characterization of CNs. An appropriate experimental method is the surface enhanced Raman scattering (SERS), which, owing to the resonant excitation of surface plasmons in a suitable metallic substrate operates with enhanced Raman signals (>1000 fold) [19]. According to the vibration calculus regarding the Raman active modes in SWNTs three spectral ranges are significant, i.e. 100-350, 1000-1700 and 1700-3000 cm^{-1}. In the first range one find the Raman bands associated with the radial breathing modes (RBM) , which do not exist in graphite. Their peaks position is related to the tube diameter according to the relation ν (cm^{-1}) = 223.75/d (nm). Bands belonging to this group are very sensitive to the excitation wavelength. The intensity of each band is enhanced when the photon energy of the excitation radiation corresponds to a transition between the van Hove singularities (E_{ii}) in the valence and conduction bands of all possible nanotubes. The second group, consisting of G and D bands, covers the interval from 1000 to 1700 cm^{-1}. These bands are not only related to the nanotube structure: the former, peaking at about 1595 cm^{-1} , usually called as G, is a complex band attributed to the tangential vibration mode (TM). Recent data describe the G complex band as being formed from two bands noted as G^+ and G^- , which in the case of the metallic SWNTs are attributed to the transversal optic (TO)-circumferential and longitudinal optic (LO) -axial vibration modes, respectively [20]. The D band, whose peak position varies with the excitation wavelength, is frequently associated with a disorder or defects state induced in the graphitic lattice or nanotubes. Another group, located in the high wave number range from 1700 to 3500 cm^{-1}, corresponds to the second order Raman spectrum. As a rule, the most intense bands are those detected at approximately twice the wavenumber of the D and G bands. Like their first-order counterparts, they behave resonantly when the excitation wavelength is changed.

4.2. Influence of the catalyst

Two catalysts of different catalytic metal loading 4.5%Fe:4.5%Co/MgO (78) and 2.5%Fe:1.25%Co/MgO (79) were studied in order to reduce the particle size of catalytic metal by lowering their concentrations on the support. However, as the Mössbauer spectra revealed, the Fe dispersion is much higher for 78 despite the lower loading of 79, pointing to the importance of Co and of a Co/Fe ratio close to 1 as reported [14].

The Raman spectra in Fig.3-4 of the products synthesized at 900°C on each of the two catalysts show poor quality nanotubes appeared for 79: intense D bands (defect rich) and / or amorphous carbon and no radial breathing modes (RBMs) modes at excitation with 514 nm. The better quality, RBMs at all excitations, high ratios of G/D intensities, intense 2D($G^{'}$) band, of 78-I (Fe to Co ratio 1:1) is also in agreement with the observation [14] that ratio close to 1 is favourable for SWNT(DWNT) formation.

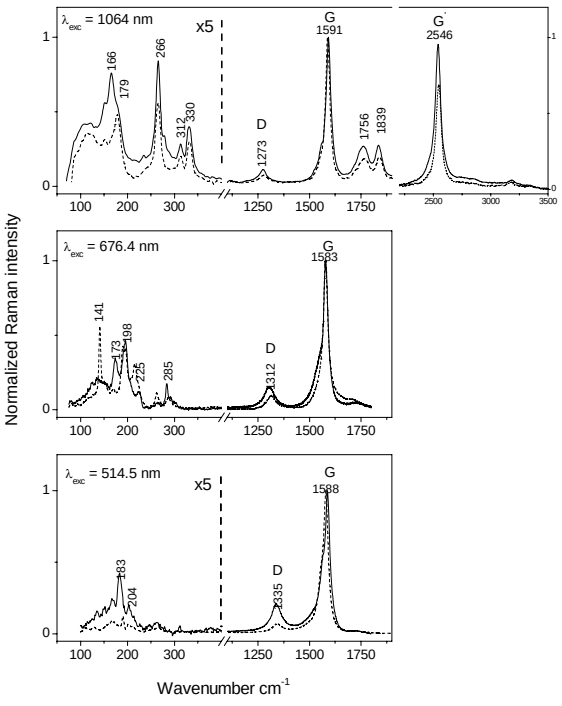

Fig. 3. Raman spectra (SERS) for nanotubes synthesized from ethanol (5 Torr) at 900°C on 4.5%Fe:4.5%Co/MgO catalyst sample 78-I (solid curves) and DWNT-Aldrich (inner tube diameter d_i=1.3 nm) for comparison (dashed curves)

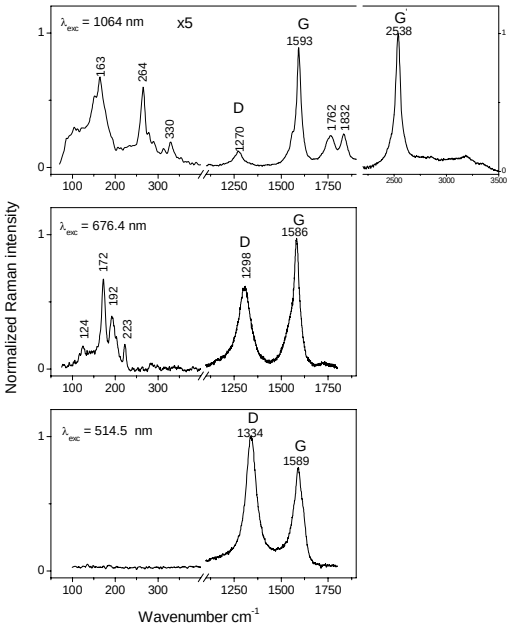

Fig.4 Raman spectra (SERS) for nanotubes synthesized from ethanol (5 Torr) at 900°C on .5%Fe:1.25%Co/MgO catalyst (sample 79).

The dominant diameters for 78-I are found in the ranges 0.7-0.9; 1.2-1.5 and 2-2.3 nm.

A method for evaluation the DWNTs content in a SWNTs/DWNTs mixture, based on the fact that 2D band splits in two bands for DWNTs, was proposed [24]. The FWHM at 514 nm excitation and 633 nm of the 2D band in the table above are significantly higher than 50-60 cm^{-1} for pure SWNTs [24,25] which suggest a significant amount of DWNTs in 78.

The spectra of 78-I, 78-II (78-I subjected to a second purification by heating in air to 500°C with 5°C/min followed by Soxhlet extraction) or 78-III (78-I heated in air saturated with water vapour for 24 h at 280°C) closely resemble the Aldrich DWNTs as shown in Fig.5. However, the treatments in acid show that for 78-II all the RBMs corresponding to nanotube diameters between 0.7 and 2.3 nm strongly decrease in intensity while for Aldrich DWNTs, the bands at 264, 315, 331 cm^{-1} remain almost unchanged, as expected for inner nanotubes. This suggests that the amount of DWNTs in 78 is lower as compared to Aldrich DWNTs

Table 3. RBM bands observed for the sample 78-I, the diameters calculated by $\omega_{RBM}=224/d+14$ (left) or $\omega_{RBM}=223.75/d$ and the nanotube type according to Kataura diagram.

λ_{laser}	RBM bands [cm^{-1}]	Diameter [nm]		Type
1064 nm	100-120	2-2.4	1.9-2.2	metallic
SERS	166 i	1.47	1.35	semiconductor
	266 i	0.95	0.84	semiconductor
	312;330 m	0.71-0.75	0.68-0.72	semiconductor
676,4 nm	125 w	2.0	1.79	semiconductor
SERS	173 vi	1.51	1.37	metallic
	198 vi	1.22	1.13	metallic
	285 w	0.83	0.79	semiconductor
633 nm	130 (145.8) w	1.82 – 1.93	1.53-1.72	
micro Raman	189 vi	1.28	1.18	semiconductor
$2D_{FWHM}=80$ cm^{-1}	213 vi	1.12	1.05	metallic
				metallic
514 nm	183 i	1.33	1.22	semiconductor
SERS	204 m	1.18	1.1	metallic
	265 w	0.95	0.84	metallic
514 nm	140-156w	1.58-1.78	1.43-1.6	semiconductor
micro Raman	170m	1.43	1.32	semiconductor
$2D_{FWHM}=88$ cm^{-1}	185vi	1.31	1.21	semiconductor
	248-267m	0.88-0.96	0.85-0.9	metallic

vi=very intense; i=intense; m=moderate; w=weak; vw=very weak

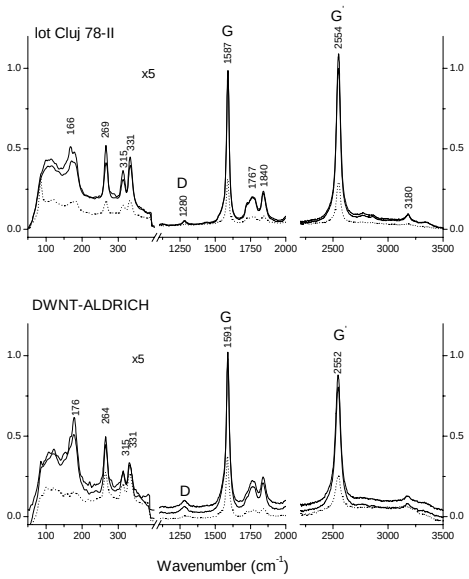

Fig. 5 Transformation of 78-II and DWNT-ALDRICH carbon nanotubes by a chemical treatment with an acid and base solution. The thick solid lines illustrate the initial states, the dashed spectra were obtained plugging the samples for 15 min. in 0.5M H2SO4 solution and the thin solid lines show the recovered states after the sample immersion for 10 min. in 0.5M KOH solution.

4.3 Synthesis conditions - effects at the interface with carbon source

Aiming to an increased content of DWNTs, syntheses in other conditions were performed on the same catalyst, as given in Table 4. The residence time $\tau=\rho V/G$ of the ethanol on the catalyst was calculated as in [23] but for a volume V=1 cm^3 of the reaction tube, taking into account the ethanol density ρ in the total feed mass flow rate G (ethanol and argon) . The I_G/I_D ratios of 80, 80b show an increased quality (high I_G/I_D ratios) of the nanotubes and a significant increase of all the RBMs at 1064 nm in Fig.6, the spectra resembling closely to those of Aldrich DWNTs from Fig.5 and also of other high quality DWNTs reported in literature [24,25].

Tentatively, the histogram given in Fig.7, based on the Raman spectra may be used for a comparative analysis of the products. As compared with the low pressure (5 Torr ethanol) conditions, where the sum of the all nanotube diameters in the range 0.7-1nm correspond to a fraction ~0.23, for 80 and 80b the fraction (resulting from the histogram in Fig.7) of diameters in this range increases to 0.52-0.54. Thus in argon flow and low residence time about half of the nanotubes are found within this range. The increase of the low diameter nanotubes with the decreasing partial pressure of hydrogen is in perfect agreement with the effect of increasing the catalytic Fe particle size in the presence of hydrogen reported by Ago *et al*. [13].

Table 4. Residence time for various CCVD conditions for nanotube synthesis from ethanol at 900°C on 4.5%Fe:4.5%Co/MgO in quartz tube of 18 mm inner diameter.

Sample	Synthesis conditions	Residence time τ [s]	I_G/I_D 1064nm 676.4mm 514.5nm	Partial pressure of H_2 resulting from ethanol [Torr]
78	5 Torr ethanol 0.027 g ethanol/min	0.067	14 3.4	11
80	Argon flow 170 sccm/min (10.5 sccm/min through ethanol)	0.0045	20 11 9	8
80b	Argon flow 300 sccm/min (10.5 sccm/min through ethanol)	0.0014	16 5 13	3.3

The partial pressure of H_2 evaluated from ethanol equilibrium thermodynamics [17]

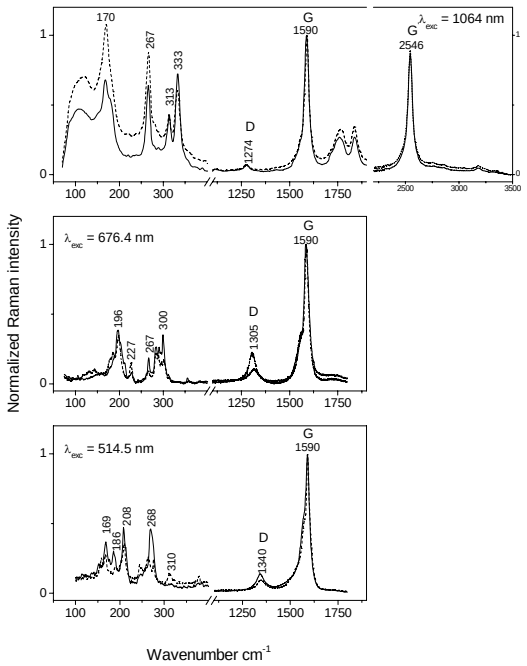

Fig. 6. Raman spectra (SERS) for nanotubes synthesized from ethanol at 900°C on 4.5%Fe:4.5%Co/MgO catalyst in argon flow 170 sccm argon for the sample 80 (solid curve) and 300 sccm for 80b (dashed curve)

The close resemblance of the Raman spectra for 80 and 80b with Aldrich DWNTs, suggests that the DWNT content increases for CCVD performed in argon flow at the atmospheric pressure. Two possible pairs of tubes satisfying the condition of diameter difference 0.67-0.82nm may be identified as corresponding to DWNTs: with 0.7 and, respectively 1.4nm as inner tubes and outer tubes of 1.4 and, respectively, 2-2.3nm diameters.

As concerning the role of hydrogen, it was revealed that reactive H species, unavoidably arising in CCVD with carbon sources containing hydrogen [26], the small diameter tubes are preferentially attacked by reactive H species during CCVD, finally resulting in larger diameter SWNTs. This is also in agreement with the results in the series 78-80-80b: as the partial pressure of hydrogen is lower, a significant increase of low diameter tubes (d<1 nm) can be observed in the histogram for 80, 80b as compared to 78. Selective syntheses from ethanol on mixed Fe/Co catalysts reported that "SWNTs synthesized on the iron-rich catalyst have narrow diameters" [27].

For Fe-Co alloys the hyperfine field increases with their Co content and the B_{eff} values from Table 1 supply experimental evidence on the presence of different magnetic phases encapsulated in 78-I nanotubes. From the histogram, the fraction of tubes of three dominant diameter ranges 0.7 – 1 , 1.1 – 1.5 and 2 – 2,3 nm are 0.24, 0.61 and 0.15 respectively and they may not be co-related with only two types of Fe-Co observed. It is interesting to note that a ratio of the two Fe-Co alloys with different B_{eff} encapsulated in nanotubes 78-I is close to 1:2 (32.1: 62.3), the theoretical ratio of metallic to semiconducting nanotubes [18]. A detailed discussion [28] of the intermediate stages involved in CCVD process emphasizes that the reconstructive nucleation at the *catalytic metal nanoparticles/carbon nanotubes interface* causes structural and magnetic phase changes during the stage of melting and reconstruction of metal nanoparticles, which modulate the carbon nanotubes growth. Further Mössbauer studies on the encapsulated metal resulting from different catalysts and synthesis conditions might give additional information in this direction.

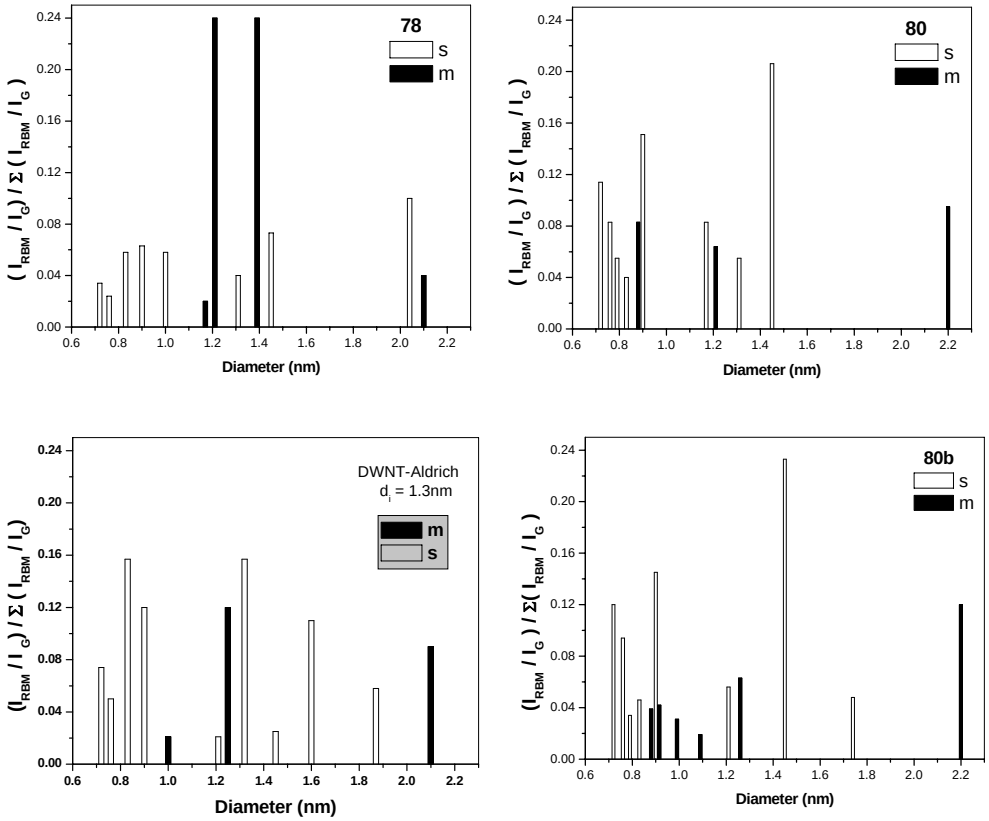

Fig. 7. A histogram based on $(I_{RBM}/I_G)/(\text{sum } I_{RBM}/I_G)$ vs. the tube diameter for the samples 78, 80 and 80b and Aldrich DWNTs (d_i=1.3nm) . The sum refers to all the RBM peaks observed in the Raman spectra at 1064, 676.4 and 514.5 nm. Open bars refer to semiconductor and filled bars to metallic nanotubes according the Kataura diagrams.

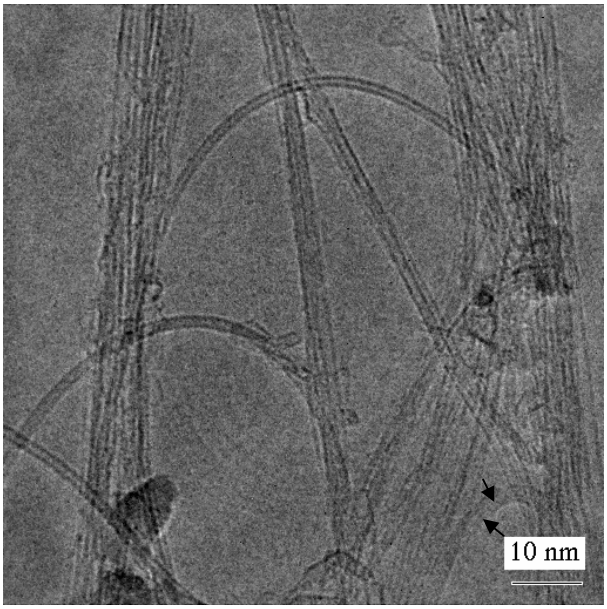

Fig. 8. TEM image for nanotubes synthesized at 900°C, 5 Torr ethanol, 15 min on Fe4.5%:Co4.5%:MgO in graphite boat. Mostly SWNTs of 1-1.3 nm diameter are present and a DWNT in the bottom right corner marking with arrows the outer and inner tubes.

In Fig.8 the TEM image shows indeed that CCVD in vacuum results in a rather low content of DWNTs, a single double-walled tube can be clearly identified.

5. Conclusions

1. Mössbauer spectroscopy studies of Fe-Co/MgO catalysts proved that a high dispersion degree of Fe may be achieved for catalysts with Fe/Co ratio close to 1. They also showed that the presence of hydrogen at high temperatures increases the particle size of catalytic Fe.

2. The reduced iron species (Fe^{2+} and metallic Fe-Co alloy) resulting from highly oxidized species of Fe^{3+} inside the catalysts can be quantitatively evaluated from their areas in the Mössbauer spectra of catalyst reduced for short time with hydrogen. This may be a measure of the readiness to reduction of a given catalyst, depending on the initial degree of iron dispersion.

3. The nanotube yields for two catalysts with rather different (Fe,Co) concentrations are proportional to the amount of (Fe-Co alloy + Fe^{2+}) which occur in the catalyst after a short time reduction with hydrogen. This relationship is in pretty good agreement with the mechanisms proposed in literature [13,14] pointing out to the importance of these two species in balancing the growth process of SWNTs(or DWNTs).

4. The Raman spectra show that the carbon nanotubes synthesized from ethanol in argon flow on 4.5%Fe:4.5%Co/MgO are abundant in low diameter (0.7-1.0nm) tubes than those obtained at low ethanol pressure. This is in agreement with the effects generated by hydrogen, reported in literature, both on the catalyst [13,14] and on nanotubes [26]: i) as the partial pressure of hydrogen (resulting from ethanol decomposition at 900°C) decreases, there are less favourable conditions for an increase of catalytic metal particle size by additional reduction of iron species to metal [13] and ii) preferential availability of small diameter tubes to attract reactive H species. The close similarity with the Raman spectra of Aldrich and literature DWNTs suggest that syntheses in argon flow at short residence time (low ethanol flux) are more favourable for the formation of double-walled nanotubes on this catalyst type.

5. Two different non equivalent sites were found in Fe-Co alloys encapsulated in carbon nanotubes. Their ratio is very close to the theoretical ratio of metallic to semiconducting nanotubes 1:2. It is premature to conclude that the two types of nanotubes grow on Fe-Co particles with different magnetic characteristics. However, this supplies experimental evidence for the presence of different magnetic phases and their implication in the stages of CCVD, in agreement with the importance of these phase changes emphasized in literature [28].

References

[1] S. Maruyama, R. Kojima, Y. Miyauchi, S. Chiashi, M. Kohno, Chem Phys Lett **360**, 229 (2002).
[2] Y. Murakami, S. Yamakita, T. Okubo, S. Maruyama, Chem Phys Lett **375**, 393 (2003).
[3] T. Okazaki, H. Shinohara, Chem Phys Lett **376,** 606 (2003).
[4] Y. Murakami, Y. Miyauchi, S. Chiashi, S. Maruyama, Chem. Phys Lett. **374**, 53 (2003).
[5] S. Maruyama, Y. Murakami, Y. Shibuta, Y. Miyauchi, S. Chiashi, J. Nanosci Nanotech, **4**, 360 (2004).
[6] A. Okamoto, H. Shinohara, Carbon **43,** 431 (2005).
[7] S. Maruyama, E. Einarsson, Y. Murakami, T. Edamura, Chem Phys Lett **403,** 320 (2005).
[8] S. Inoue, T. Nakajima, Y. Kikuchi, Chem. Phys. Lett. **406**, 184 (2005).
[9] E. Flahaut, R. Bacsa, Peigney, Laurent Ch. Chem. Commun. 1442-1443 (2003).
[10] H. Muramatsu, T. Hayashi, Y. A. Kim, M. Endo, M. Terrones, M. S. Dresselhaus, J. Nanosci Nanotech **5**, 404 (2005).
[11] E. Flahaut, A. Peigney, Ch. Laurent, A. Rousset, J. Mater. Chem. **10,** 249 (2000).
[12] M. Boudart, A. Delbouille, J. A. Dumesic, S. Khammanouma, H. Topsoe,. J. Catal. **37,** 486 (1975).
[13] H. Ago, K. Nakamura, N. Uehara, M.Tsuji, J. Phys. Chem. **B108**, 18908 (2004).
[14] P. Coquay, A. Peigney, E. De Grave, E. Flahaut, R. E. Vandenberghe, C. Laurent, J. Phys. Chem. B **109**, 17813 (2005).
[15] D. Lupu, A. R. Biriş, A. Jianu, C. Bunescu, E. Burkel, E. Indrea, G. Mihăilescu, S. Pruneanu, L. Olenic, I. Mişan, Carbon **42,** 503 (2004).
[16] A. R. Biriş, A. S. Biriş, D. Lupu, S. Trigwell,

E. Dervishi, Z. Rahman, P. Mărginean, Chem. Phys. Lett.**429**, 204 (2006).
[17] K. Vasudeva, N. Mitra, P. Umasankar, S. C. Dhingra. Int J Hydrogen Energy **21**, 13 (1996)
[18] M. S. Dresselhaus, P. C. Eklund, Phonons in carbon Nanotubes, Adv. Phys.**49,** 705 (2000).
[19] S. Lefrant, I. Baltog, M. Baibarac, J. Schreiber, Chauvet O. Phys.Rev.B **65**, 235401 (2002).
[20] S. Piscanec, M. Lazzeri, J. Robertson, A. C. Ferrari, F. Phys. Rev. B**75,** 035427 (2007).
[21] Y. A. Kim, H. Muramatsu, M. Kojoma, T. Hayashi, M. Endo, M. Terrones, M. S. Dresselhaus, Chem.Phys.Lett. **420,** 377 (2006).
[22] R. Pfeiffer, H. Kuzmany, F. Simon, S. N. Bokova, E. Obraztsova, Phys. Rev. B**71**, 155409-1-8 (2005).
[23] R. Brukh, S. Mitra, Chem. Phys. Lett. **424**, 126 (2006).
[24] A Grüneis, M. H. Rümmeli, C. Kramberger, A. Barreire, T. Pichler, R. Pfeiffer, H. Kuzmany, T. Gemming, B. Büchner, Carbon **44,** 3177 (2006).
[25] S. C Lyu, B. C. Liu, S. H. Lee, C. Y. Park, H. K. Kang, C. W. Yang, C. J. Lee, J Phys Chem B **108**, 2192 (2004).
[26] G. Zhang, D. Mann, L. Zhang, A. Javey, Y. Li, E. Yenilmez, Q. Wang, J. P. McVittie, Y. Nishi, J. Gibbons, H. Dai Ultra-high-uield growth of vertical single-walled carbon nanotubes: Hidden roles of hydrogen and oxygen. PNAS 2005;102:16141-16145. www.pnas.org/cgi/doi/ 10.1073/pnas.0507064102
[27] S. Inoue, Y. Kikuchi, Chem. Phys. Lett.**410**, 209 (2005).
[28] R B. Little, Mechanistic Aspects of Carbon Nanotube Nucleation and Growth. J Cluster Sci. **14**, 135.

*Corresponding author: filoti@infim.ro